The Fermi surface of $ErGa_3$

1999 J. Phys.: Condens. Matter 11 4507

(http://iopscience.iop.org/0953-8984/11/23/305)

J. Phys.: Condens. Matter **11** (1999) 4507–4516. Printed in the UK PII: S0953-8984(99)01874-3

The Fermi surface of $ErGa_3$

V B Pluzhnikov†‡, A Czopnik§‖ and G E Grechnev‡

† International Laboratory of High Magnetic Fields and Low Temperatures, Gajowicka 95, 53-529 Wrocław, Poland
‡ B Verkin Institute for Low Temperature Physics and Engineering, 47 Lenin Avenue, Khar'kov 310164, Ukraine
§ W Trzebiatowski Institute of Low Temperature and Structure Research, PO Box 1410, 50-950 Wrocław, Poland

E-mail: czopnik@int.pan.wroc.pl

Received 16 February 1999

Abstract. The Fermi surface geometry and cyclotron masses of the antiferromagnet $ErGa_3$ in a magnetic-field-induced paramagnetic phase are determined by using the de Haas–van Alphen effect method. The results are analysed on the basis of *ab initio* band-structure calculations and compared to corresponding results for the isostructural compounds $TmGa_3$ and $LuGa_3$.

1. Introduction

In the present work we continue our recent [1, 2] studies on the electronic structure of the cubic $REGa_3$ (RE: heavy rare-earth metal) compounds. The primary aim of this work is the determination of the Fermi surface (FS) geometry and effective cyclotron masses of the $ErGa_3$ compound by means of the de Haas–van Alphen (dHvA) effect.

Information on physical properties of $ErGa_3$ is scarce. This compound crystallizes in the cubic $AuCu_3$-type structure with the lattice constant $a = 4.212$ Å. The compound orders antiferromagnetically at $T_N = 2.8$ K through a continuous transition, and the magnetic structure, determined at 2.1 K, appeared to be the incommensurate sinusoidally modulated one (see reference [3]). One may expect—and we are going to show later—the compound to reveal a large and strong field-dependent magnetization. This brings about, as in the case of $TmGa_3$ [2], a number of difficulties in the Fourier analysis of dHvA oscillations. As a result, one has to study the dHvA effect in sufficiently strong magnetic fields, where the magnetization tends to saturate. Obviously, these fields are higher than the critical field destroying the antiferromagnetic order. Therefore, dHvA effect study of $ErGa_3$ is possible in the paramagnetic phase, in which the magnetic field leads to a ferromagnetic configuration (not *state*) of magnetic moments.

In this work, the experimental study is supplemented by *ab initio* band-structure calculations, which give more details of the spin-polarized electronic structure of $ErGa_3$. The dHvA effect data, complemented with the results of the calculations, provide the possibility of estimating the many-body enhancement of the 'bare' cyclotron masses. The electronic structure parameters evaluated are compared to results obtained for the isostructural compounds $TmGa_3$ and $LuGa_3$.

‖ Author to whom any correspondence should be addressed.

0953-8984/99/234507+10$19.50

2. Experiment

Single crystals of $ErGa_3$ were grown by the flux method from a melt of the nominal composition 90 at.% Ga plus 10 at.% Er. The purities of the starting metals were 6N for Ga and 4N for Er. The feed, placed in an alumina crucible and sealed in a quartz tube in an argon atmosphere under a pressure of 150 Torr at room temperature, was heated in a resistance furnace up to 920 °C, held at this temperature for 48 h, and then slowly cooled down at the rate 0.8 K h^{-1}. The synthesis was stopped at about 350 °C and then the sample was cooled quickly down to room temperature to avoid the formation of $ErGa_6$ in a peritectic reaction [4]. The resulting crystals of $ErGa_3$ were immersed in an excess of Ga, which is easy to remove. The crystals obtained had the form of cubes with maximum dimensions $5 \times 5 \times 5$ mm^3. According to the x-ray examination, the quality of the single crystals was very good.

The dHvA effect measurements were performed on a spherical sample (diameter 2.5 mm) by using the standard field-modulation technique at temperatures down to 1.5 K and in magnetic fields up to 15 T. In order to investigate the angular dependence of the dHvA frequencies, the sample can be rotated. This allowed us to carry out the measurements for magnetic fields in the [100] and [110] planes.

The Fourier analysis of the dHvA oscillations was performed by taking into account the magnetic induction $\boldsymbol{B} = \boldsymbol{H}_{\text{appl}} + (8\pi/3)\boldsymbol{M}$. Complementary magnetization measurements were carried out using a home-made vibrating-sample magnetometer. The magnetic phase diagram was determined on the basis of the magnetization measured using a SQUID magnetometer (Quantum Design). The field dependences of the magnetization along the ⟨001⟩, ⟨110⟩, and ⟨111⟩ axes are shown in figure 1. For other directions, the field dependence of the magnetization has been calculated self-consistently in the molecular-field approximation. The Hamiltonian employed contains the crystal field (CF), the exchange, and Zeeman terms. The molecular-field exchange parameter was estimated, on the basis of the value of the paramagnetic Curie temperature, $\Theta_p = -10$ K. This value of Θ_p was determined from the temperature dependence of the paramagnetic susceptibility measured using the SQUID magnetometer.

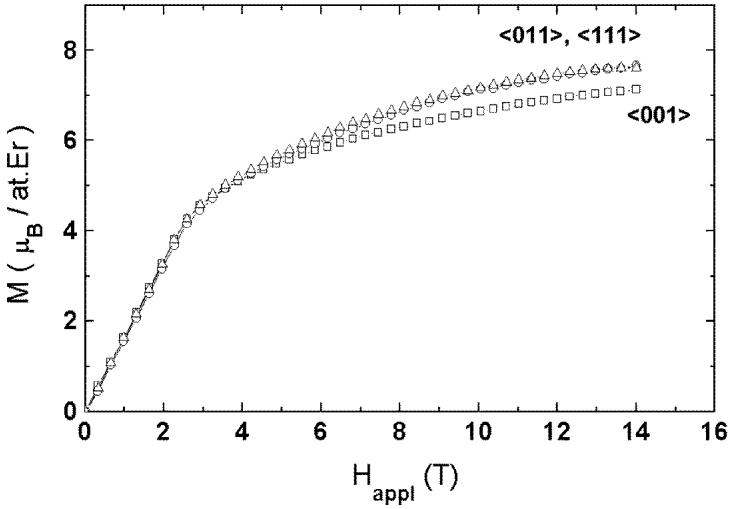

Figure 1. The field dependence of the magnetization of $ErGa_3$ at 1.7 K along the ⟨001⟩, ⟨110⟩, and ⟨111⟩ axes.

Then the best fit to the experimental data was obtained for the CF parameters x and W (in the usual notation of reference [5]) equal to 0.22 and 0.25 K, respectively. Then the CF ground state is the Γ_7 doublet, and the first excited state, the $\Gamma_8^{(1)}$ quartet, lies at about 30 K, and the overall CF splitting is about 120 K. Therefore, the calculated values of the magnetization, normalized to the experimental ones along the principal crystallographic axes, were used in the Fourier analysis of the dHvA oscillations.

The dHvA effect measurements were carried out in a paramagnetic state in magnetic fields higher than 8 T, well above the $H_c(T)$ line of the antiferromagnetic–paramagnetic transitions. The magnetization in these fields tends to saturate, and magnetic moments settle into a quasi-ferromagnetic configuration. Moreover, the magnetization is temperature independent along all directions in these fields in the temperature range 1.7–4.2 K (figure 2). For the sake of illustration, the magnetic phase diagram is shown in figure 3 for the field applied along the ⟨001⟩ axis. The estimated critical field, H_c, destroying the antiferromagnetic order, reaches a value close to 3 T at 0 K. Along other directions, H_c does not exceed this value. This diagram shows that in the antiferromagnetically ordered state, several phases occur. At low temperatures, in zero magnetic field, the magnetic structure is a sinusoidally modulated one. Above 2.6 K, the magnetic structure changes due to the rotation of the magnetic moments. The full description of this diagram, together with the neutron diffraction results, will be presented elsewhere [6].

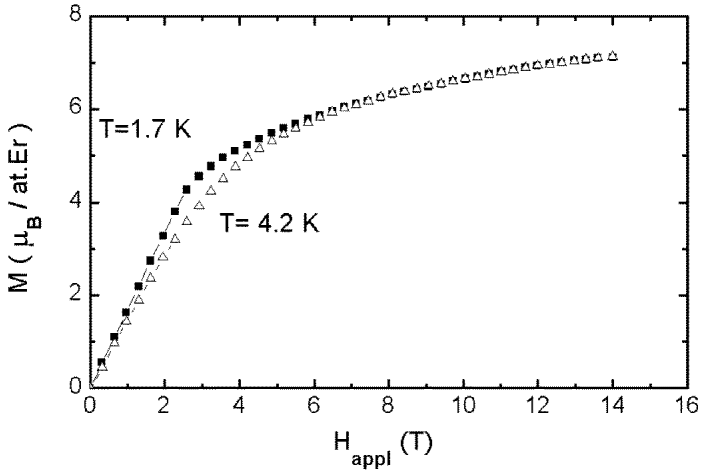

Figure 2. The field dependence of the magnetization of $ErGa_3$ at 1.7 K and 4.2 K along the ⟨001⟩ axis.

For the intensity range employed, a magnetic field induces a quasi-ferromagnetic configuration of magnetic moments. When this configuration is attained, the magnetization does not change distinctly, and Fourier analysis of the dHvA oscillations can be performed. In another case, the dHvA frequencies would change in value following the strength of the external magnetic field. Also, for the field-induced quasi-ferromagnetic configuration, the dHvA spectrum of $ErGa_3$ can be compared with the results of the band-structure calculations for the spin-polarized state.

The effects of the antiferromagnetic ordering on the Fermi surface of $ErGa_3$ have not been examined in this research. For this phase, the large magnetization and its strong dependence on the magnetic field have prevented us from analysing the dHvA oscillations.

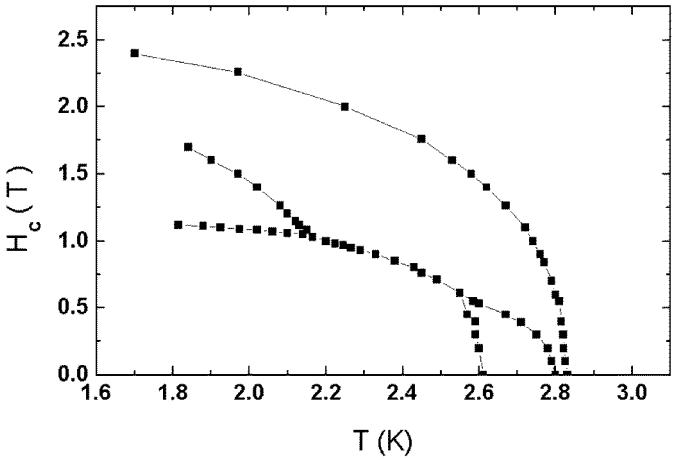

Figure 3. The magnetic phase diagram of $ErGa_3$ for the magnetic field applied along the ⟨001⟩ axis. The upper curve is the line representing the phase transition between the antiferromagnetic state and the paramagnetic one.

3. Theory

It is commonly believed [7–9] that within the local spin-density approximation (LSDA) a treatment of heavy rare-earth 4f states as bands is suitable for Gd and its compounds only when the seven filled spin-up 4f states lie below, and the empty spin-down f states above the Fermi energy (E_F). But even for Gd, the calculated 4f bands appear to be too close to E_F in comparison to those of experimental photoemission spectra (see references [10–12]), and the hybridization with other conduction electron states is apparently too large, raising the state density at E_F and leading to an unenhanced electronic specific heat coefficient which is larger than the measured value. The situation is far worse for other rare-earth metals, since in spin-polarized calculations a spin shell is not filled and the 4f bands, which act as a sink for electrons, always cut the Fermi level leading to absurd values of the specific heat coefficients [7] and incorrect 4f occupancies, close to the divalent (i.e. atomic) configuration [12].

Test band-structure calculations for Gd and Er pnictides were carried out in reference [9] within the LSDA, treating the 4f states as bands, as well as the localized core states. By comparing the results of these calculations with a wealth of experimental data (including data on bulk and FS properties), solid evidence has been obtained that a strict band treatment for the 4f states is inadequate for heavy rare earths.

According to the photoemission data [10–12], the 4f spectral density for Er and Er-based compounds was observed about 5 eV below E_F. Therefore, for the present purpose, which is mainly to describe the band structure for the trivalent ground state near E_F, it seems reasonable to treat 4f states as semilocalized core states, as is done in references [7–9, 13, 14]. The bulk and magnetic properties, as well as Fermi surfaces, of Tb [8] and ErAs [9] calculated within the same approach appeared to be in agreement with experimental data.

In this work, the standard rare-earth model [7] is employed in the limit of large Hubbard repulsion U within the *ab initio* LSDA scheme [15] for the exchange–correlation effects. The problem of handling the localized f states of Er was solved according to the method outlined in references [13, 14]. Namely, the spin occupation numbers were fixed by applying the Russell–Saunders coupling scheme to the 4f shell. Therefore, the 4f states were not allowed

to hybridize with conduction electrons. They were treated as spin-polarized outer-core wave functions, contributing to the total spin density, but not being part of the band structure.

The self-consistent band-structure calculations were carried out for the paramagnetic configuration phase of $ErGa_3$ by using the linear muffin-tin orbital method (LMTO) in the atomic sphere approximation (ASA) with combined corrections to the ASA included [16, 17]. In the framework of the LSDA, the spin density of the 4f states polarizes the spin-up and spin-down conduction electron states through the local exchange interaction. The exchange-split conduction electron states interact with the localized f states at other sites, appearing as the medium for the indirect f–f interaction [14].

In order to calculate FS orbits, the converged charge densities were obtained by including spin–orbit coupling at each variational step, as suggested in references [7, 8]. In this case the spin is no longer a good quantum number, and it is not possible to evaluate the electronic structure for 'spin-up' and 'spin-down' bands separately. Also, we have employed the standard approximation, which has been extremely successful for rare earths [7], namely, that of omitting spin–orbit coupling in the spin-polarized band-structure calculations for $ErGa_3$. This provides the possibility of elucidating the role of the spin–orbit coupling, and also of presenting 'spin-up' and 'spin-down' bands for the field-induced ferromagnetic configuration phase of $ErGa_3$, where the exchange splitting is much larger than the spin–orbit coupling.

The self-consistent band-structure calculations were performed on a uniform mesh of 455 points in the irreducible wedge of the cubic Brillouin zone for the experimental lattice constant value. The individual atomic radii of the components were chosen following the general rule, proposed in reference [18]. We have checked the results of the LMTO-ASA calculations by comparing them with those from our own full-potential LMTO calculations for selected high-symmetry lines, and we found that the electronic structures and shapes of the FS are similar in the two types of calculation.

The calculated partial densities of states (DOS) $N(E)$ for the ferromagnetic configuration phase of $ErGa_3$ are shown in figure 4. There are two fairly broad peaks (bonding and antibonding states) arising due to hybridization of 5d states of Er and p states of Ga. As can be seen in figure 4, these p states give a substantial contribution to the total DOS at the Fermi energy. On the other hand, the exchange splitting is more pronounced for the 5d states of Er due to the local exchange interaction.

4. Results and discussion

The angular dependences of the dHvA frequencies in the (100) and (110) planes for $ErGa_3$ are shown in figure 5. The dHvA frequencies and corresponding cyclotron masses along the principal crystallographic axes, $\langle 100\rangle$, $\langle 110\rangle$, and $\langle 111\rangle$, are given in table 1.

The intersections of the calculated FS of $ErGa_3$ with the high-symmetry planes of the Brillouin zone (figure 6) reveal the 'spin-split' seventh-band electron FS centred at the R point and the sixth-band hole FS centred at the Γ and X points, analogously to the cases for $LuGa_3$ and $TmGa_3$ [1, 2]. As a whole, the electron FS of $ErGa_3$ is nearly spherical, whereas the hole FS is a complicated multiply connected surface.

As seen in figure 5, the agreement between the results of the *ab initio* FS calculations and experimental data is quite good in the range of the high dHvA frequencies (branch a, related to the FS sheet at the R point, and branch d, associated with the largest sheet of the hole FS centred at the Γ point), as well as the intermediate ones (branch b, related to the hole FS sheet at the X point). Not seen in the experiment, however, are dHvA oscillations from 'spin-split' subbands. On the basis of the calculated partial DOS (see figure 4), one can expect more readily observed dHvA oscillations related to the majority states, having lower DOS,

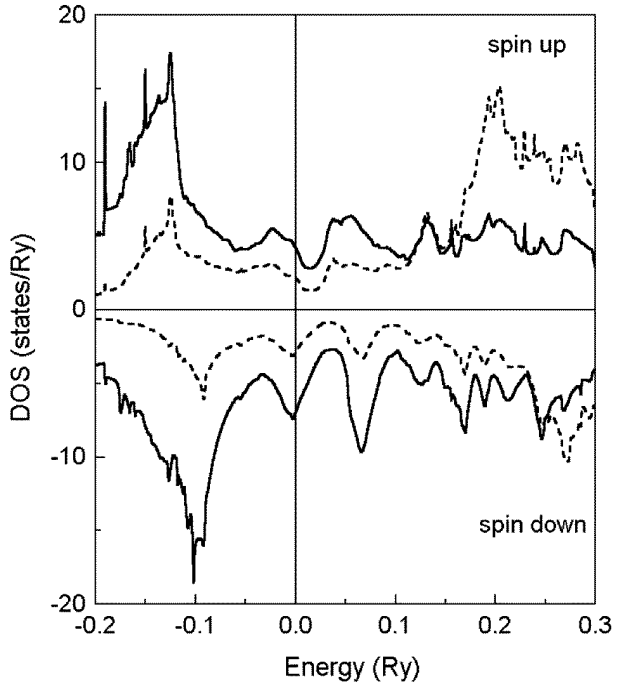

(a)

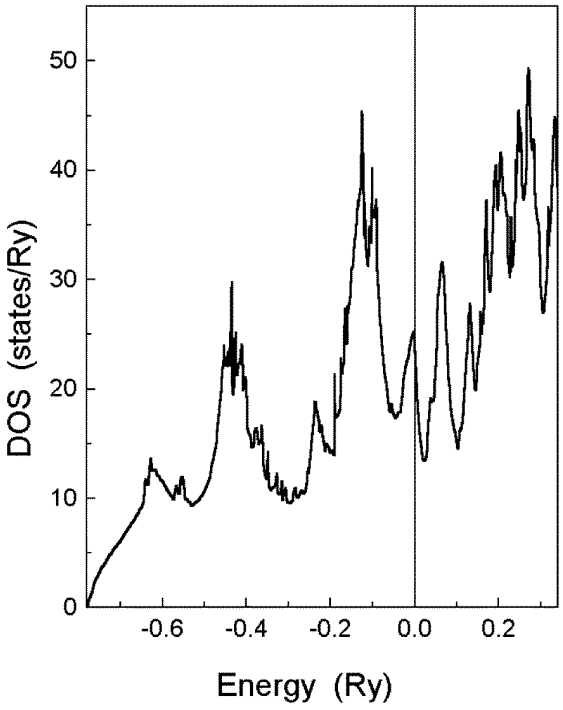

(b)

Figure 4. Calculated densities of states as functions of energy (relative to the Fermi energy) for the ferromagnetic configuration phase of $ErGa_3$. (a) Partial densities; solid curves stand for p states of Ga, and dashed curves represent 5d states of Er. (b) The total density of states.

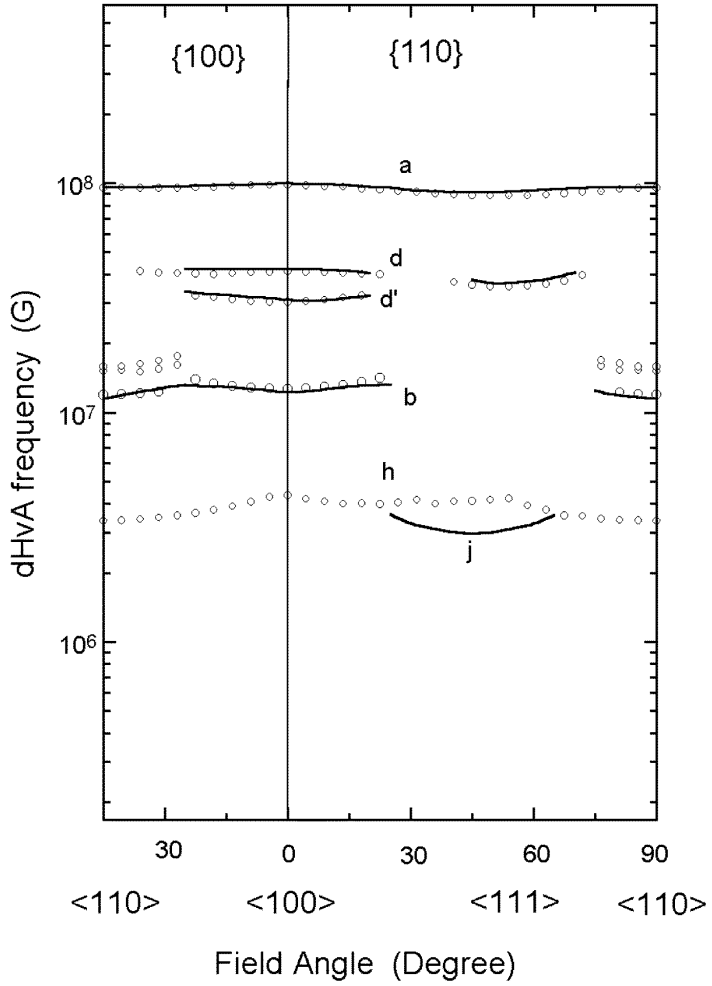

Figure 5. The angular dependence of the dHvA frequencies in $ErGa_3$. Circles stand for the experimental data; solid curves show calculated results.

Table 1. dHvA frequencies and the corresponding cyclotron masses (experimental, m_c^*, and calculated, m_c^b, in units of the free-electron mass) for $ErGa_3$.

⟨100⟩			⟨110⟩			⟨111⟩		
F (10^6 G)	m_c^*	m_c^b	F (10^6 G)	m_c^*	m_c^b	F (10^6 G)	m_c^*	m_c^b
98.17	0.96 ± 0.02	0.40	95.57	0.89 ± 0.02	0.37	88.14	0.80 ± 0.02	0.37
41.07	0.91 ± 0.02	0.46				35.47	0.70 ± 0.02	0.40
30.27	0.92 ± 0.03							
			15.80					
			15.14	0.57 ± 0.02				
12.66	0.44 ± 0.02		11.95	0.84 ± 0.04				
4.35	0.55 ± 0.02		3.37	0.28 ± 0.02		4.21	0.51 ± 0.02	

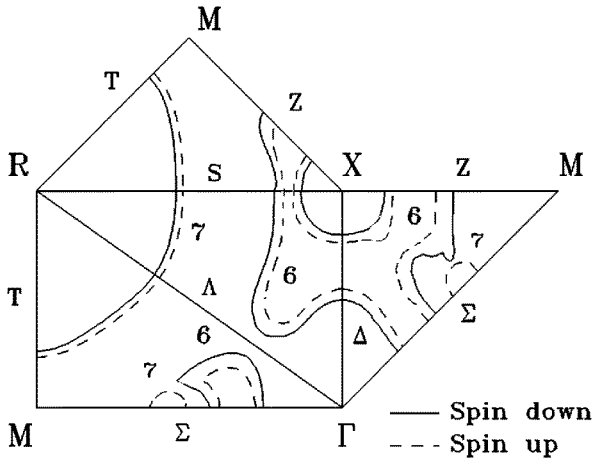

Figure 6. The intersection of the Fermi surface for $ErGa_3$ with the Brillouin zone planes for 'spin-up' and 'spin-down' bands. '6' and '7' are band numbers.

and, correspondingly, lower band masses. In fact, the frequencies calculated for 'spin-up' bands (which are actually presented in figure 5) appeared to be in much better agreement with the experimentally observed ones. In the range of the low dHvA frequencies, instead of the calculated branch j, originating from a 'neck' at the symmetry line ΓR, there is a branch with a different angular field dependence, labelled h in figure 5, and analogous to a branch previously found for $LuGa_3$ [1, 2].

The dHvA spectrum of $ErGa_3$ in the field-induced ferromagnetic configuration is very close to the spectrum of the paramagnet $LuGa_3$ [1]. The only difference is the presence of an additional branch d′ in the spectrum of $ErGa_3$ that is just below the d branch and located around the ⟨100⟩ axis. The dHvA spectrum observed for $TmGa_3$ [2] differs from the $ErGa_3$ spectrum in that it contains several h-like branches in the low-dHvA-frequency range and no d′ branch.

Glancing at the experimental lattice parameters, which are very close for $ErGa_3$ and $TmGa_3$, one may assume that the crystal potentials in the two compounds do not differ substantially. The differences between the $TmGa_3$ and $ErGa_3$ spectra are most probably due to the different behaviours of the ground-state $^3H_6$ and $^4I_{15/2}$ multiplets of the Tm^{3+} and Er^{3+} ions in the CFs of $TmGa_3$ and $ErGa_3$, respectively. The triplet $\Gamma_5^{(1)}$ [3] is the ground state in $TmGa_3$ and most probably Γ_7 is the ground state in the CF of $ErGa_3$. Since the $\Gamma_5^{(1)}$ state exhibits a quadrupolar moment and the Γ_7 state does not, one can expect large magnetostriction effects in $TmGa_3$ and none in $ErGa_3$. Also, in the quasi-ferromagnetic configuration of the magnetic moments, the exchange splitting of the conduction bands can vary in $ErGa_3$ and $TmGa_3$ due to the difference in the corresponding 4f-shell spin occupation numbers. Unfortunately, one cannot attribute in an unambiguous way the differences in angular dependences of dHvA frequencies in $REGa_3$ either to the conduction band splitting or to the magnetostriction. In order to elucidate this problem we have undertaken studies of the pressure effect on the Fermi surfaces and electronic structures of $ErGa_3$ and $LuGa_3$. The initial results of these studies can be found in reference [19].

Cyclotron masses have been determined for all dHvA frequencies in the field applied along the ⟨100⟩, ⟨110⟩, and ⟨111⟩ axes, and appeared to be smaller than the free-electron mass.

Band cyclotron masses have been calculated for the a and d branches, and are also presented in table 1. The mass enhancement factor λ, which is defined in terms of experimental, m_c^*, and calculated, m_c^b, cyclotron masses by the relation $m_c^* = m_c^b(1 + \lambda)$, is a measure of the strength of interaction of the conduction electrons with low-energy excitations.

In table 2 a comparison is given of λ-factors for electrons in a and d orbits in $ErGa_3$, $TmGa_3$ [2], and $LuGa_3$ [2]. In the case of non-magnetic $LuGa_3$, the λ-factor is expected to be a measure of the electron–phonon interactions, whereas in $ErGa_3$ and $TmGa_3$ this factor also contains a contribution arising from the interactions of conduction electrons with magnetic excitations. As can be seen in table 2, for the $LuGa_3$ compound the λ-factor ranges from 0.3 (for the d branch) to about 1 (for the a branch). These values are in agreement with the independent estimate of the averaged electron–phonon λ_{e-ph}, resulting from McMillan's relation [20] for superconducting $LuGa_3$ ($T_c = 2.35$ K): $\lambda_{e-ph} \simeq 0.6$. On the assumption that the values of λ_{e-ph} for $REGa_3$ are close to the corresponding ones for $LuGa_3$, one can estimate the additional magnetic contributions λ_{mag} in $ErGa_3$ to be within the ranges 0.4–0.6 and 0.4–0.7 for the a and d orbits, respectively. For $TmGa_3$ the corresponding values of λ_{mag} appear to be larger and more anisotropic, namely 0.5–1 and 0.8–1.5. The CF scheme for $TmGa_3$ gives a $\Gamma_5^{(1)}$ ground state with intrinsic magnetic and quadrupolar moments. Therefore, the enhancement factor, λ, determined from comparison of the experimental cyclotron effective masses with the corresponding calculated ones, presumably contains a contribution from coupled magnetic quadrupolar excitations.

Table 2. Comparison of the mass enhancement factors λ for $REGa_3$ compounds.

		λ		
Branch	Orientation	$ErGa_3$	$TmGa_3$*	$LuGa_3$*
a	⟨100⟩	1.4	1.93	0.95
a	⟨110⟩	1.4	1.68	1.03
a	⟨111⟩	1.16	1.02	0.58
d	⟨100⟩	0.98	1.83	0.31
d	⟨111⟩	0.75	1.14	0.36

* Taken from reference [2].

It was shown in references [21–23] that virtual magnetic excitations can contribute substantially to the effective mass of the conduction electrons in rare-earth systems. These excitations are magnetic excitons in paramagnetic systems (e.g. praseodymium), and spin waves in magnetically ordered rare earths. The mass enhancement appeared to be large, magnetic field dependent, and proportional to the static susceptibility of the magnetic system. According to estimations of the electronic specific heat coefficients, performed in reference [22], the corresponding effective masses increase in the series of heavy rare-earth metals. This trend is in accord with the observed cyclotron masses in $ErGa_3$ and $TmGa_3$, but considerable work is needed to employ the theory developed in reference [22] to obtain a quantitative description of the experimentally observed differences in cyclotron masses.

In principle, the hybridization with 4f states could also contribute to the cyclotron masses observed in $ErGa_3$ (and $TmGa_3$) being larger than those in $LuGa_3$, and affect the shape of the FS as well. In this case a strong hybridization with 4f bands would lead to substantial reduction of the conduction bandwidth in $REGa_3$ and thus to remarkably different bulk properties in comparison to those of $LuGa_3$. According to the behaviour of the experimental lattice parameters, which decrease slightly in a linear fashion in the series $ErGa_3$, $TmGa_3$, and $LuGa_3$ due to the lanthanide contraction, we can expect, however, the conduction bandwidths to be

very close for $REGa_3$, and the 'bare' cyclotron masses should also be close.

In conclusion, we admit that more work is needed to elucidate the nature of the large cyclotron masses observed in $REGa_3$, and, in particular, to evaluate the effects of coupling to magnetic quadrupolar and CF excitations. Also, the hybridization with 4f states should be taken into consideration as well in the framework of a rigorous version of the LSDA + U method or some other Hubbard-like approach. As was shown in section 3, the hybridization effects are somewhat overestimated within the LSDA. At the present stage, even calculations within some LSDA + U scheme would not be of decisive importance, and more elaborate analysis is necessary to estimate the scale of the hybridization effects. These tasks clearly go beyond the scope of the present paper, in which we tried to reach a true LSDA limit within the standard rare-earth model in order to explain the experimental dHvA data.

Acknowledgments

We are grateful to Professor J Klamut and Professor I V Svechkarev for their kind support. This work was performed within the research programme of the Polish Committee for Scientific Research, KBN Nr2 P302 091 06.

References

[1] Pluzhnikov V B, Czopnik A and Svechkarev I V 1995 *Physica* B **212** 375
[2] Pluzhnikov V B, Czopnik A, Grechnev G E, Savchenko N V and Suski W 1999 *Phys. Rev.* B **59** 7893
[3] Morin P, Giraud M, Regnault P L, Roudaut E and Czopnik A 1987 *J. Magn. Magn. Mater.* **66** 345
[4] Pelleg J, Kimmel G and Dayan D 1981 *J. Less-Common Met.* **81** 33
[5] Lea K R, Leask M J M and Wolf W P 1962 *J. Phys. Chem. Solids* **23** 1381
[6] Murasik A, Czopnik A, Keller L and Fischer P 1999 *J. Magn. Magn. Mater.* submitted
[7] Brooks M S S and Johansson B 1993 *Ferromagnetic Materials* vol 7, ed K H J Buschow (Amsterdam: North-Holland) p 139
[8] Ahuja R, Auluck S, Johansson B and Brooks M S S 1994 *Phys. Rev.* B **50** 5147
[9] Petukhov A G, Lambrecht W R L and Segall B 1996 *Phys. Rev.* B **53** 4324
[10] Herbst J F and Wilkins J W 1987 *Handbook on the Physics and Chemistry of Rare Earths* vol 10, ed K A Gschneidner Jr, L Eyring and S Hufner (Amsterdam: North-Holland) p 321
[11] Freeman A J, Min B I and Norman M R 1987 *Handbook on the Physics and Chemistry of Rare Earths* vol 10, ed K A Gschneidner Jr, L Eyring and S Hufner (Amsterdam: North-Holland) p 165
[12] Min B I, Jansen H J F, Oguchi T and Freeman A J 1986 *J. Magn. Magn. Mater.* **61** 139
[13] Brooks M S S, Nordstrom L and Johansson B 1991 *Physica* B **172** 95
[14] Grechnev G E, Panfilov A S, Svechkarev I V, Buschow K H J and Czopnik A 1995 *J. Alloys Compounds* **226** 107
[15] von Barth U and Hedin L 1972 *J. Phys. C: Solid State Phys.* **5** 1629
[16] Andersen O K 1975 *Phys. Rev.* B **12** 3060
[17] Skriver H L 1984 *The LMTO Method* (Berlin: Springer)
[18] Andersen O K, Jepsen O and Sob M 1987 *Electronic Band Structure and Its Applications* ed M Yussouff (Berlin: Springer) p 1
[19] Pluzhnikov V B, Czopnik A, Eriksson O, Grechnev G E and Fomenko Yu V 1999 *Low Temp. Phys.* submitted
[20] McMillan W L 1968 *Phys. Rev.* **167** 331
[21] White R M and Fulde P 1981 *Phys. Rev. Lett.* **47** 1540
[22] Fulde P and Jensen J 1983 *Phys. Rev.* B **27** 4085
[23] Fulde P and Loewenhaupt M 1986 *Adv. Phys.* **34** 589